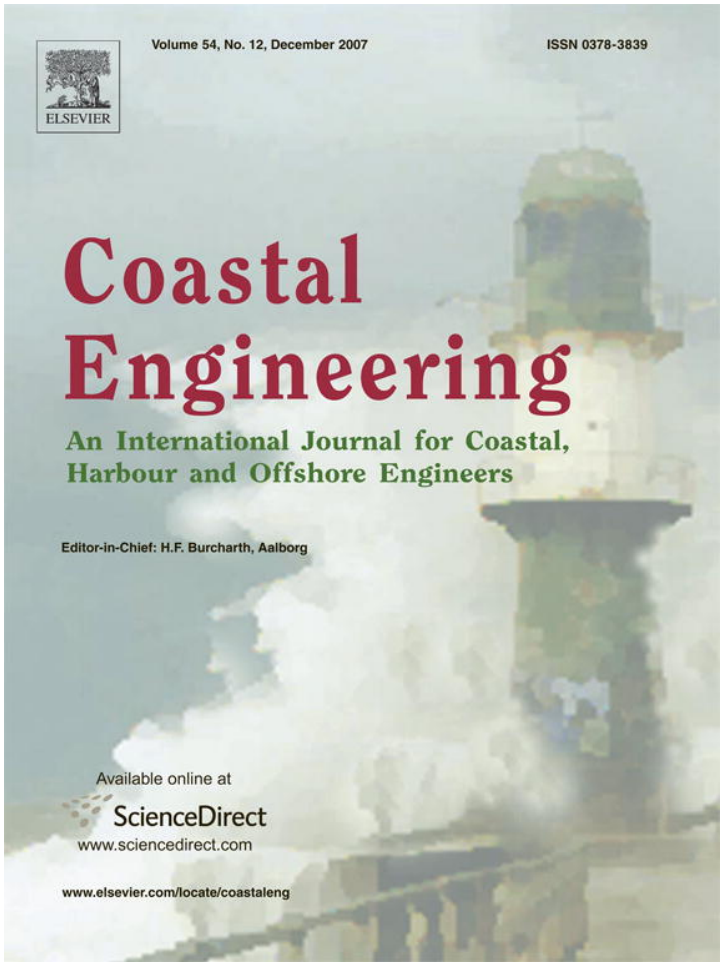

Available online at www.sciencedirect.com
ScienceDirect
Coastal Engineering 54 (2007) 914–929
Coastal Engineering
An International Journal for Coastal, Harbour and Offshore Engineers
www.elsevier.com/locate/coastaleng

Seabed shear stress and bedload transport due to asymmetric and skewed waves

David Gonzalez-Rodriguez *, Ole Secher Madsen

R.M. Parsons Laboratory, Department of Civil and Environmental Engineering, Massachusetts Institute of Technology, Cambridge, MA 02139, USA

Received 31 March 2007; received in revised form 26 June 2007; accepted 28 June 2007
Available online 13 August 2007

Abstract

A simple conceptual formulation to compute seabed shear stress due to asymmetric and skewed waves is presented. This formulation generalizes the sinusoidal wave case and uses a variable friction factor to describe the physics of the boundary layer and to parameterize the effects of wave shape. Predictions of bed shear stresses agree with numerical computations using a standard boundary layer model with a k–ε turbulence closure. The bed shear stress formulation is combined with a Meyer-Peter and Müller-type formula to predict sheet flow bedload transport under asymmetric and skewed waves for a horizontal or sloping bed. The predictions agree with oscillatory water tunnel measurements from the literature.

Keywords: Seabed shear stress; Boundary layer; Sediment transport; Bedload modeling; Wave asymmetry; Wave skewness

1. Introduction

Onshore sediment transport under waves remains largely unexplained. While undertow and bottom slope effects are the principal agents for offshore transport, several physical mechanisms for onshore transport have been identified (see discussion by Henderson et al., 2004). Among these mechanisms, the effect of fluid accelerations associated with the shape of nearshore waves seems to play a key role (e.g., Nielsen, 1992; Drake and Calantoni, 2001; Hoefel and Elgar, 2003; Hsu and Hanes, 2004; Calantoni and Puleo, 2006).

Nearshore waves are asymmetric and skewed. A wave with *positive* asymmetry has a forward-leaning shape, with a steep frontal face and a gentle rear face. A wave with *positive* skewness has a peaked, narrow crest and a flat, wide trough. Nearshore waves have both positive asymmetry and skewness. As waves shoal, they first become skewed. Once waves approach breaking and enter the surf zone, they become strongly asymmetric.

Based on experimental observations of asymmetric waves by King (1991), Nielsen (1992, Section 2.4.4) identified the importance of fluid acceleration in asymmetric waves. For a forward-leaning wave, the onshore velocity increases in magnitude faster than the offshore velocity, and the associated boundary layer has a shorter time to develop. Thus, the onshore velocity generates a thinner boundary layer and therefore a larger bed shear stress. To account for this effect, Nielsen (1992) proposed an empirical formula that sets the Shields parameter to be a sum of two terms. One term is a function of the near-bed (free-stream) velocity and the other is a function of the near-bed acceleration. The weighting of each term is determined by an adjustable model parameter. Sediment transport is calculated using Meyer-Peter and Müller's (1948) bedload formula. Modifications of the Shields parameter formula were later introduced by Nielsen (2002), to account for the turbulent behavior of the boundary layer, and by Nielsen and Callaghan (2003), to account for boundary layer streaming. In a recent contribution, Nielsen (2006) calibrates the model parameter so that his sediment transport predictions agree with the asymmetric laboratory wave data by Watanabe and Sato (2004).

Drake and Calantoni (2001) carried out computationally intensive discrete particle simulations of sheet flow transport in

* Corresponding author. Room 48-216-13. Tel.: +1 617 253 1691; fax: +1 617 258 8850.
E-mail addresses: davidgr@alum.mit.edu (D. Gonzalez-Rodriguez), osm@mit.edu (O.S. Madsen).

0378-3839/$ - see front matter © 2007 Elsevier B.V. All rights reserved.
doi:10.1016/j.coastaleng.2007.06.004

oscillatory flows, which supported a different interpretation of the fluid acceleration effects. According to their interpretation, differences in acceleration between the front and the back of an asymmetric wave yield horizontal pressure gradients in the boundary layer, which act on the near-bed fluid and sediment. To describe this effect, they suggested the use of an acceleration skewness parameter, $a_{spike}=\langle a^3\rangle/\langle a^2\rangle$, where a is the time series of the near-bed fluid acceleration and the angle brackets denote a time average. Using this acceleration descriptor, Hoefel and Elgar (2003) modified Bailard's (1981) sediment transport model to include a term that accounts for fluid accelerations and used this model to successfully predict an episode of onshore bar migration. However, to achieve agreement with observations, Hoefel and Elgar adjusted the acceleration parameters by a factor of 5 relative to the values originally suggested by the discrete particle model of Drake and Calantoni (2001).

Several studies of nearshore sediment transport rely on intensive numerical simulations, such as discrete particle models (e.g., Drake and Calantoni, 2001; Calantoni and Puleo, 2006), k–ε turbulence boundary layer models (e.g., Henderson et al., 2004; Holmedal and Myrhaug, 2006), and two-phase models (e.g., Hsu and Hanes, 2004; Liu and Sato, 2006). While these detailed models provide valuable understanding of the nearshore transport processes, they are too computationally demanding for most practical applications.

This paper presents a simple conceptual model to compute bed shear stress under asymmetric and skewed waves. The model is physically based, free of adjustable parameters, and computationally efficient. The model is described in Section 2 and validated against a computationally intensive standard boundary layer model with a k–ε turbulence closure in Section 3. As Hsu and Hanes (2004) concluded, sediment transport of coarse grains (which is bedload dominated) can be accurately parameterized in terms of the seabed shear stress. Therefore, accurate prediction of the bed shear stress suffices to compute bedload. In Section 4, predictions of bedload under asymmetric and skewed waves based on our conceptual model are compared with laboratory measurements in the sheet flow regime. In Section 5, we discuss the potential contribution of suspended transport to the total transport.

2. Conceptual model of the seabed shear stress

The maximum bed shear stress under sinusoidal waves, τ_{bm}, can be written as (Jonsson, 1966)

$$\tau_{bm}=\frac{1}{2}\rho f_{ws}u_{bm}^2, \tag{1}$$

where ρ is the water density, f_{ws} is the wave friction factor for sinusoidal waves, and u_{bm} is the maximum near-bed wave orbital velocity. For symmetric and non-skewed waves, f_{ws} is assumed a constant determined by wave and sediment characteristics. Based on the linearized boundary layer equations and assuming a time-invariant, linearly varying eddy viscosity, Madsen (1994) obtained an implicit equation for f_{ws}. According to Madsen (1994), the solution of this equation can be approximated by the following explicit formulas:

$$f_{ws}=\begin{cases}\exp(7.0X^{-0.078}-8.8) & \text{for } 0.2<X<10^2\\ \exp(5.6X^{-0.109}-7.3) & \text{for } 10^2<X<10^4\end{cases} \tag{2}$$

with $X=u_{bm}/(k_N\omega)$, where k_N is the equivalent Nikuradse sand-grain roughness of the bed, and ω is the wave radian frequency. The phase shift between the bed shear stress and the near-bed wave orbital velocity, ϕ_τ (in radians), can be approximated by (Madsen, 1994)

$$\phi_\tau=\frac{\pi}{60}(11-2.0\log_{10}X)\quad \text{for } 0.2<X<10^3. \tag{3}$$

Often, (1) is generalized to describe the instantaneous bed shear stress, $\tau_b(t)$, as a function of the instantaneous near-bed wave orbital velocity, $u_b(t)$ (e.g., Madsen and Grant, 1976; Ribberink, 1998; Hsu et al., 2006):

$$\tau_b(t)=\frac{1}{2}\rho f_{ws}u_b(t+l_\tau)|u_b(t+l_\tau)|, \tag{4}$$

where $l_\tau=\phi_\tau/\omega$ is the time lag between the bed shear stress and the near-bed velocity.

In this paper, we extend this formulation to asymmetric and skewed waves. The profile of the corresponding near-bed orbital velocity, $u_b(t)$, is characterized by the parameters u_c, u_t, T_c, T_t, T_{cp}, and T_{tn}, as illustrated in Fig. 1.

To extend (4) to asymmetric and skewed waves, the friction factor must vary with time. Otherwise, a purely asymmetric wave with zero skewness would lead to a non-skewed bed shear stress and yield zero net bedload transport, which contradicts observations (e.g., Watanabe and Sato, 2004). The use of a variable friction factor over the wave period is justified by examining the physics of the boundary layer.

Consider the near-bed orbital velocity of an asymmetric and skewed wave, $u_b(t)$, represented in Fig. 1. When the near-bed orbital velocity turns onshore (point B), a wave boundary layer starts to develop. To be precise, this development starts slightly before B, due to the time lag between $\tau_b(t)$ and $u_b(t)$. By neglecting the velocity history before the zero velocity at B, the development of the boundary layer from B to C can be assumed

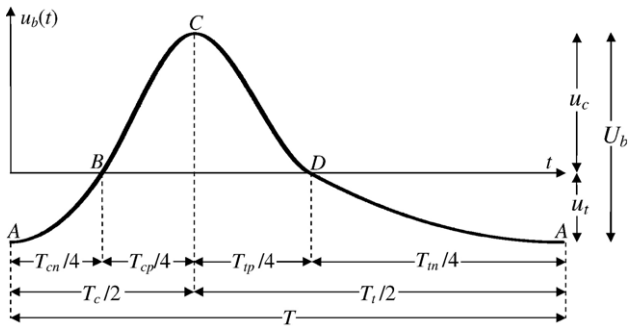

Fig. 1. Near-bed wave orbital velocity of an asymmetric and skewed wave. Positive velocity is directed onshore.

similar to that induced by a quarter period of a sinusoidal wave of velocity amplitude u_c and period T_{cp}. Therefore, the maximum shear stress near the wave crest can be approximated by

$$\tau_{b,max} = \frac{1}{2}\rho f_{ws,c} u_c^2, \tag{5}$$

where $f_{ws,c}$ is the friction factor corresponding to a sinusoidal wave of period T_{cp} and velocity amplitude u_c. This friction factor is given by (2) with $X=(u_c T_{cp})/(2\pi k_N)$. Similarly, the phase shift at the crest, $\phi_{\tau,c}$, can be approximated using (3). The corresponding time lag is $l_{\tau,c}=\phi_{\tau,c}T_{cp}/(2\pi)$.

When the near-bed orbital velocity changes direction again (point D) the boundary layer associated with the onshore velocity disappears. However, shortly before this happens, a new boundary layer associated with the negative near-bed orbital velocity starts to develop. Analogous to (5), the minimum shear stress near the wave trough can be approximated by

$$\tau_{b,min} = -\frac{1}{2}\rho f_{ws,t} u_t^2, \tag{6}$$

where $f_{ws,t}$ is the friction factor corresponding to a sinusoidal wave of period T_{tn} and velocity amplitude u_t. The friction factor, $f_{ws,t}$, and the phase shift, $\phi_{\tau,t}$, are given by (2) and (3), respectively, with $X=(u_t T_{tn})/(2\pi k_N)$. The time lag is $l_{\tau,t}=\phi_{\tau,t}T_{tn}/(2\pi)$.

The bed shear stress over the wave cycle is then approximated by

$$\tau_b(t) = \frac{1}{2}\rho f_w(t) u_b(t + l_\tau(t))|u_b(t + l_\tau(t))|, \tag{7}$$

where the time-varying friction factor, $f_w(t)$, and the time-varying lag, $l_\tau(t)$, are assumed to be the linear interpolation in time between the values calculated at the wave crest ($f_{ws,c}$ and $l_{\tau,c}$) and trough ($f_{ws,t}$ and $l_{\tau,t}$).

The application of this simple conceptual model to predict bed shear stresses of real waves relies on our ability to estimate the shape of $u_b(t)$. In particular, it is necessary to estimate the parameters u_c, u_t, T_c, T_{cp}, and T_{tn}, represented in Fig. 1. From the results of numerical simulations using a Boussinesq model, Tajima and Madsen (2002) developed a set of relationships that predict four of these five parameters as a function of the local water depth, bottom slope, wave height, and period. The only parameter not provided by Tajima and Madsen's relationships is T_{tn}, but this parameter can be estimated by assuming a shape of the near-bed orbital velocity constrained by the four known parameters plus the zero net flux condition. Recently, Elfrink et al. (2006) derived a set of empirical formulas that yield all five parameters as a function of the same local characteristics as Tajima and Madsen's (2002) relationships.

3. Numerical model of the boundary layer

To assess the accuracy of the conceptual model presented in Section 2, we compare its bed shear stress predictions with those of a numerical model of the boundary layer with a k–ε turbulence closure. The numerical model, here applied to the simple case of periodic waves with no mean current, is similar to Holmedal et al.'s (2003) model.

3.1. Governing equations

To the leading order of approximation, the momentum equation in the turbulent wave boundary layer reads

$$\frac{\partial u}{\partial t} = \frac{\partial u_b}{\partial t} + \frac{\partial}{\partial z}\left(\frac{\tau_{zx}}{\rho}\right), \tag{8}$$

where $u(z,t)$ is the horizontal velocity, $u_b(t)$ is the near-bed (free-stream) wave orbital velocity, and z is the vertical coordinate measured positively upward. The shear stress, $\tau_{zx}(z,t)$, is related to the velocity through

$$\tau_{zx} = \rho \nu_t \frac{\partial u}{\partial z}, \tag{9}$$

where ν_t is the eddy viscosity. To make the problem solvable, the eddy viscosity must be in turn related to the other variables through a closure model.

Following recent studies (Holmedal et al., 2003; Henderson et al., 2004), we adopt the k–ε model (e.g., Pope, 2000, pp. 373–382) as the closure. The transport equation for the turbulent kinetic energy, k, is

$$\frac{\partial k}{\partial t} = \frac{\partial}{\partial z}\left(\frac{\nu_t}{\sigma_k}\frac{\partial k}{\partial z}\right) + P - \varepsilon, \tag{10}$$

where $P=\nu_t(\partial u/\partial z)^2$ is the production of kinetic energy, and ε, the dissipation of kinetic energy, is governed by the transport equation

$$\frac{\partial \varepsilon}{\partial t} = \frac{\partial}{\partial z}\left(\frac{\nu_t}{\sigma_\varepsilon}\frac{\partial \varepsilon}{\partial z}\right) + c_{\varepsilon 1}\frac{P\varepsilon}{k} - c_{\varepsilon 2}\frac{\varepsilon^2}{k}. \tag{11}$$

The eddy viscosity, ν_t, is calculated as

$$\nu_t = c_\mu \frac{k^2}{\varepsilon}. \tag{12}$$

The standard values of the model constants are $c_\mu=0.09$, $c_{\varepsilon 1}=1.44$, $c_{\varepsilon 2}=1.92$, $\sigma_k=1.00$, and $\sigma_\varepsilon=1.30$. These values were recommended by Launder and Spalding (1974) for plane jets, mixing layers, and unidirectional steady flows near walls. Using these standard values, the k–ε model has been successfully applied to describe sinusoidal oscillatory flows over rough beds (e.g., Justesen, 1988) and, more recently, periodic flows due to skewed waves (Holmedal and Myrhaug, 2006). In both cases, hydrodynamical predictions agree with experimental data. Therefore, it is expected that the use of the standard k–ε model will lead to satisfactory predictions of asymmetric and skewed oscillatory flows.

3.2. Boundary conditions

Since the seabed is irregular, the definition of the bed elevation, $z=z_0$, is arbitrary. We adopt the conventional definition $z_0=k_N/30$, where k_N is the equivalent Nikuradse sand-grain roughness of the bed.

At the bed, the no-slip condition requires the velocity to vanish, i.e.,

$$u = 0 \text{ at } z = z_0. \tag{13}$$

The bed boundary conditions for k and ε are usually determined by assuming a logarithmic velocity profile and imposing equilibrium between production and dissipation of turbulent kinetic energy (e.g., Holmedal et al., 2003), which yields

$$k = \frac{\nu_t \left|\frac{\partial u}{\partial z}\right|}{\sqrt{c_\mu}} \tag{14}$$

and

$$\varepsilon = \left(c_\mu\right)^{3/4} \frac{k^{3/2}}{\kappa z_0} \tag{15}$$

at $z=z_0$. Note that, under the assumption of a logarithmic velocity profile, (14) and (15) imply

$$\nu_t = \kappa u_* z \tag{16}$$

at $z=z_0$, where κ is the Von Kármán constant (≈ 0.4), $u_* = \sqrt{|\tau_b(t)|/\rho}$ is the shear velocity, and $\tau_b(t)=\tau_{zx}(z=z_0, t)$ is the bed shear stress. Therefore, the standard bed boundary condition of the k–ε turbulence model relies on the same linear eddy viscosity hypothesis as Trowbridge and Madsen's (1984) model.

The top boundary conditions should be applied at a height equal to the thickness of the boundary layer, δ. The thickness of the boundary layer varies over the wave period, making its definition somewhat arbitrary. However, we note that the vertical scale of the potential flow above the boundary layer is much larger than the boundary layer thickness. Therefore, when modeling the boundary layer, the potential flow can be considered constant in z. The model will thus perform correctly by imposing the top boundary conditions at $z=z_1$, where $z_1>\delta$ but of the same order of magnitude. This guarantees that the boundary layer effects have vanished at the top of the domain.

An estimate of the maximum value of δ is given by the time-invariant thickness suggested by Madsen and Salles (1998):

$$\delta_{MS} = A \frac{\kappa u_{*m}}{\omega}, \tag{17}$$

where

$$A = \exp\left\{2.96\left(\frac{U_b/2}{k_N \omega}\right)^{-0.071} - 1.45\right\}, \tag{18}$$

$$u_{*m} = \sqrt{\frac{\tau_{bm}}{\rho}}, \tag{19}$$

U_b is the near-bed orbital velocity height, and $\tau_{bm}=1/2\rho f_{ws}(U_b/2)^2$, with f_{ws} as defined in (2). In the numerical model, we adopt

$$z = z_1 = 10\delta_{MS} \tag{20}$$

as the top boundary for the simulation.

The boundary conditions at $z=z_1$ are given as follows. The velocity is equal to the known near-bed wave orbital velocity, i.e.,

$$u = u_b \text{ at } z = z_1. \tag{21}$$

Following Holmedal et al. (2003), we impose a zero flux condition for k and ε, i.e.

$$\frac{\partial k}{\partial z} = 0 \text{ at } z = z_1 \tag{22}$$

and

$$\frac{\partial \varepsilon}{\partial z} = 0 \text{ at } z = z_1. \tag{23}$$

3.3. Numerical implementation

The boundary layer flow is governed by (8), (10), and (11), with the eddy viscosity defined by (12), the boundary conditions specified in Section 3.2, and a prescribed near-bed wave orbital velocity. The numerical implementation is carried out using finite difference.

For computational reasons, it is convenient to stretch the vertical coordinate, so that there are more grid nodes close to the bed, where the velocity varies rapidly with height. We apply the following log-linear stretching, suggested by Davies et al. (1988):

$$\zeta = \frac{1}{\chi}\left\{\ln\left(\frac{z}{z_0}\right) + \left(\frac{z-z_0}{z_*}\right)\right\}, \tag{24}$$

where

$$\chi = \ln\left(\frac{z_1}{z_0}\right) + \left(\frac{z_1 - z_0}{z_*}\right), \tag{25}$$

and we adopt $z_*=(z_0+z_1)/2$. With ζ taking on equally spaced values between 0 and 1, the previous transformation provides a conveniently distributed set of values of the elevation, z. As a consequence of this stretching, Δz is not constant in the finite difference grid. The nodes of the spatial discretization are referred to by the index $i=1, 2, 3, \ldots, N$.

Note that the system of differential equations, (8), (10), and (11), is nonlinear. The discretization of the nonlinear system of differential equations using a Crank-Nicholson finite difference scheme (e.g., Evans et al., 2000, pp. 54–57) yields a nonlinear system of algebraic equations. This system relates the unknown values of u, k, and ε for each node of the spatial grid at time $(j+1)\Delta t$ to the known values of the variables at time $j\Delta t$. To linearize the system, we apply Newton-Raphson's method (e.g., Press et al., 1992, pp. 372–375). In this method, the values of u, k, and ε at time $(j+1)\Delta t$ are determined through iteration, $n=1, 2, 3, \ldots$. The velocity at the spatial node i and time $(j+1)\Delta t$, $u_{i,j+1}$, is determined iteratively from

$$u^{n+1}_{i,j+1} = u^n_{i,j+1} + \delta u^n_{i,j+1}, \tag{26}$$

where $\delta u^n_{i,j+1}$ is an unknown small quantity ($\ll u^n_{i,j+1}$). The initial value for this iterative relationship is $u^1_{i,j+1}=u_{i,j}$. With (26) and similar expressions for k and ε, and neglecting

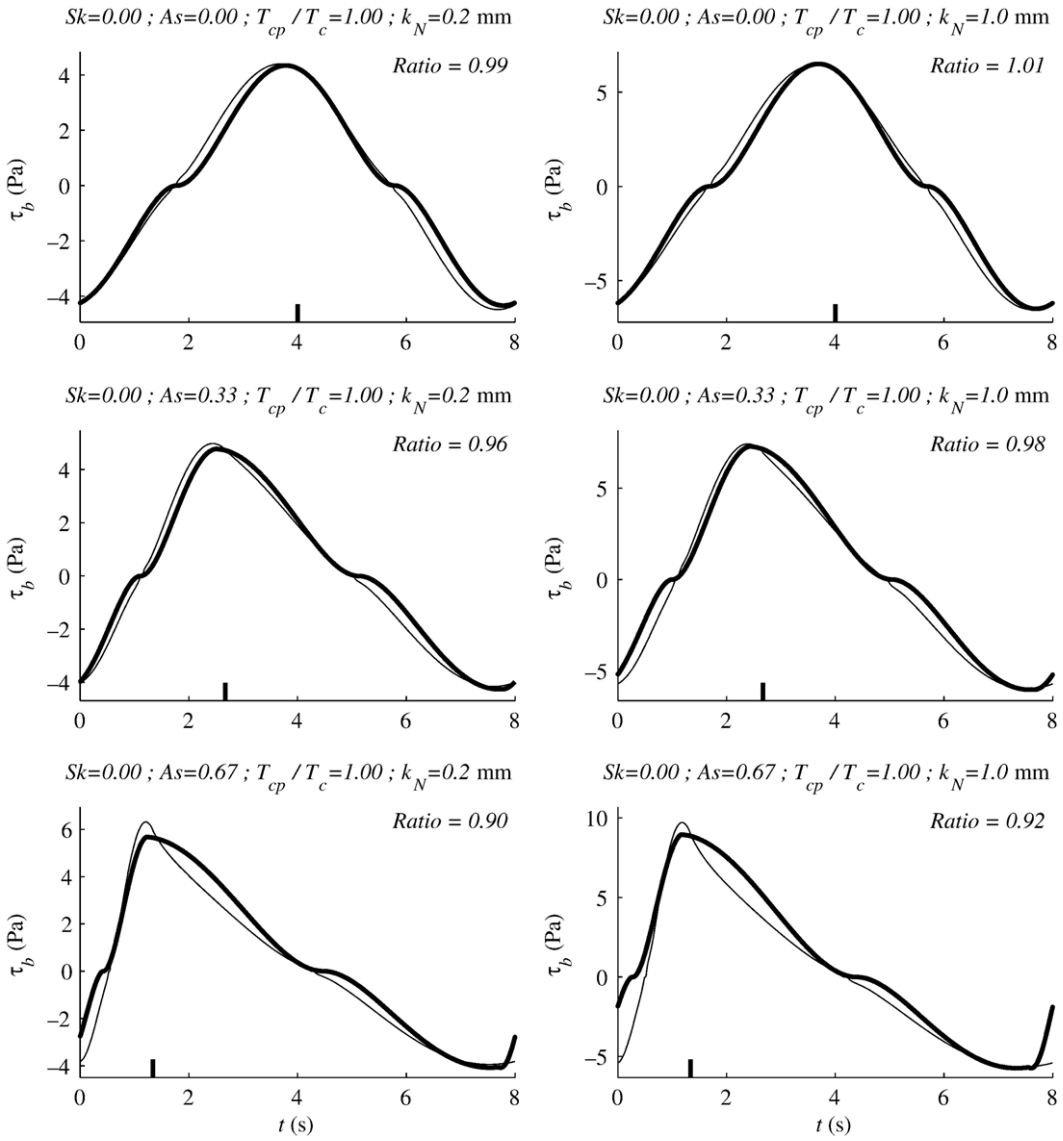

Fig. 2. Bed shear stresses predicted by the conceptual model (thick line) and the numerical model (thin line) for non-skewed waves ($Sk=0$). The ratio between maximum shear stresses predicted by the conceptual and numerical models is indicated. The tick mark on the time axis indicates the time when u_b is maximum.

products of δ-increments, we obtain a linear system of equations in the increments, which is solved for each iteration.

The initial conditions are defined at the near-bed velocity crest by assuming a log-profile steady velocity and corresponding values of k and ε. Since these initial conditions are approximate, the results for small time must be ignored. However, the code rapidly converges towards periodic conditions and yields meaningful results from the second wave period onwards.

3.4. Verification of the conceptual model

To quantify the shape of asymmetric and skewed waves, we define the asymmetry and skewness parameters as

$$As = 1 - T_c/T \tag{27}$$

and

$$Sk = 2u_c/U_b - 1, \tag{28}$$

where T_c, T, u_c, and U_b are defined in Fig. 1. With this definition, a symmetric and non-skewed wave has $As=0$ and $Sk=0$, while a forward-leaning and positively skewed wave has $0<As<1$ and $0<Sk<1$.

We compare the predictions of the bed shear stress obtained from the numerical and conceptual models for 18 test cases. All test waves are periodic, with near-bed orbital velocity height $U_b=2.5$ m/s and wave period $T=8$ s. Each test case is characterized by a specific value of the asymmetry parameter ($0 \le As \le 2/3$), the skewness parameter ($0 \le Sk \le 1/2$), and the Nikuradse sand-grain roughness of the bed (0.2 mm $\le k_N \le$ 1 mm). These ranges of As and Sk are representative of the nearshore field data compiled by Elfrink et al. (2006).

Fig. 1 illustrates the near-bed velocity profile for one of the test waves ($As=1/3$, $Sk=1/3$). The profile of each test wave, $u_b(t)$, is described by a set of two 2nd-order polynomials (between A and B and between D and A) and two 3rd-order polynomials (between B and C and between C and D). These polynomials

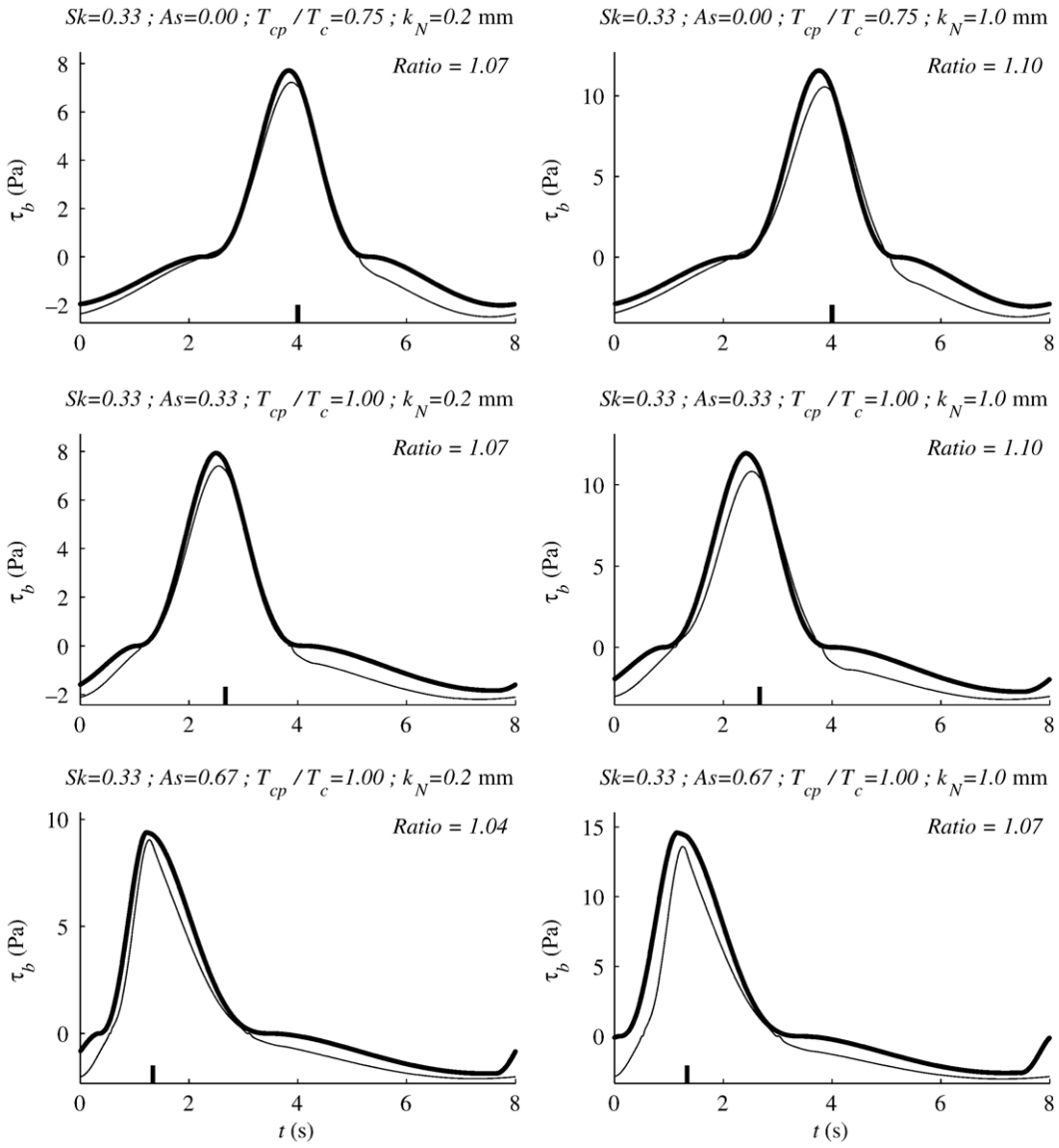

Fig. 3. Bed shear stresses predicted by the conceptual model (thick line) and the numerical model (thin line) for moderately skewed waves ($Sk=1/3$). See also caption to Fig. 2.

meet the following constraints: (i) zero derivative at A and C, (ii) continuous derivative at B and D, (iii) zero average velocity over the wave period (no mean current), and (iv) $T_{cp}=\min(T_c, T_{tp})$. In the last constraint, $T_{cp}/T_c=1$ is a characteristic value for periodic waves in the nearshore region, determined from examination of laboratory measurements of breaking periodic waves propagating over a plane sloping beach (case 6N reported by Hamilton and Ebersole, 2001). The formulas by Tajima and Madsen (2002) and Elfrink et al. (2006) yield $T_{cp}/T_c \approx 0.8–1$ and thus support our choice. To avoid a backward-leaning velocity profile in cases with large skewness and small asymmetry, we also require $T_{cp} \le T_{tp}$.

Predictions of bed shear stresses under sinusoidal waves ($As=0$, $Sk=0$) by the conceptual model overpredict the numerical results by about 10–15% for bed roughnesses of $k_N=0.2–1$ mm. This slight disagreement in the sinusoidal case is immaterial to the analysis presented here, whose purpose is to determine the ability of the conceptual model to capture the effects of asymmetry and skewness on the bed shear stress. For this reason, the numerical model is run using equivalent *numerical* roughnesses, $k'_N=0.33$ and 1.6 mm, corresponding to the physical roughnesses used for the conceptual model, $k_N=0.20$ and 1.0 mm. The *numerical* roughnesses were chosen so that both models yield the same maximum shear stresses in the sinusoidal wave cases. Note that the difference of about 60% between k_N and k'_N is of the same order of magnitude as the variability between different physical roughness estimates proposed in the literature, such as $k_N=D_{65}$ (Einstein, 1950), $k_N=2D_{65}$ (Engelund and Hansen, 1967), and $k_N=2.5D_{50}$ (Nielsen, 1992).

Figs. 2, 3, and 4 compare the bed shear stresses predicted by the conceptual model (thick lines) with the predictions of the numerical model (thin lines) for $Sk=0$, 1/3, and 1/2, respectively. Each figure shows six plots corresponding to three different values of As each for two different roughnesses. The ratio

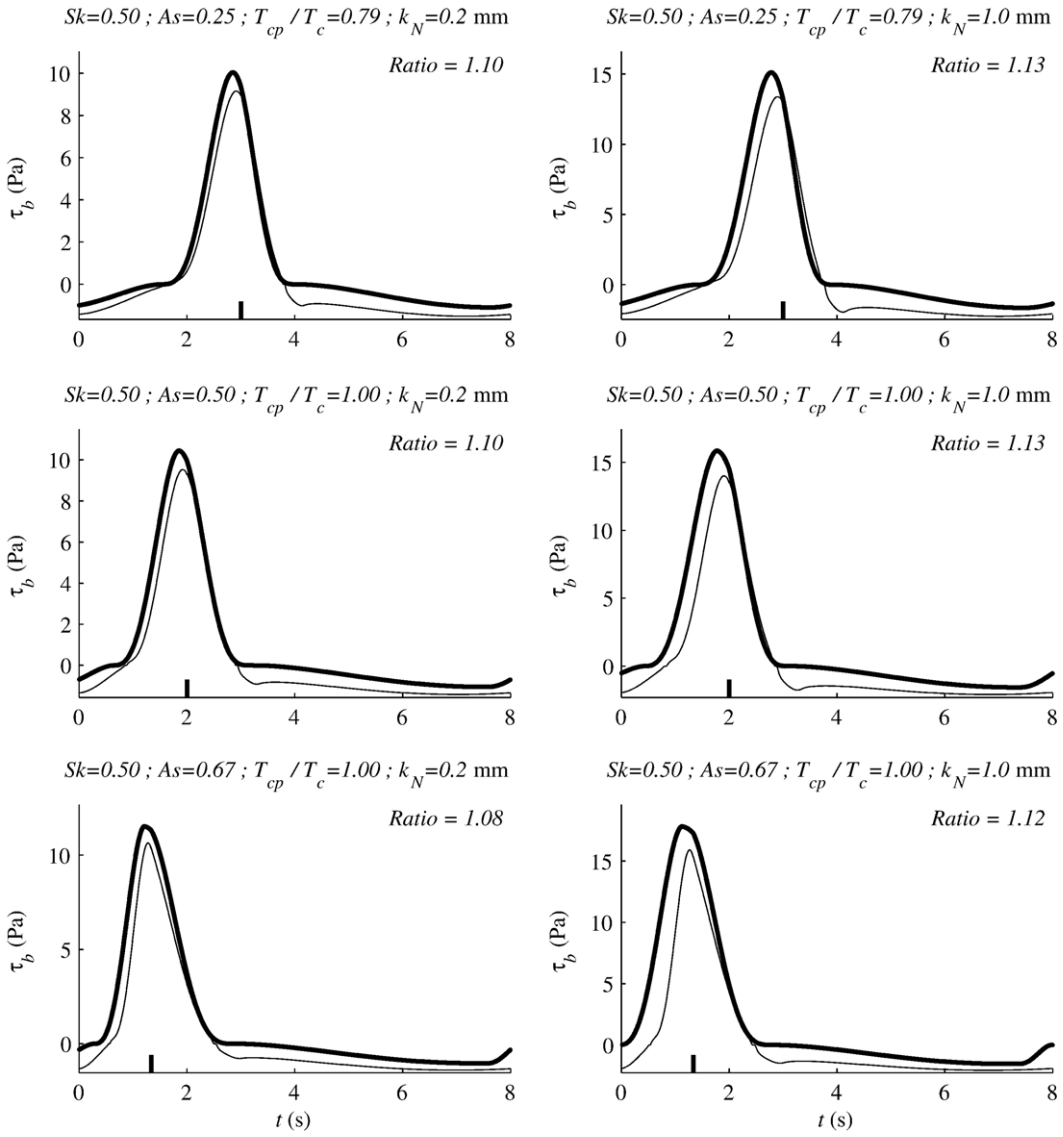

Fig. 4. Bed shear stresses predicted by the conceptual model (thick line) and the numerical model (thin line) for strongly skewed waves (Sk=1/2). See also caption to Fig. 2.

between the maximum shear stress predictions is indicated on each plot. The conceptual model captures the shape of the bed shear stresses for asymmetric and skewed waves, yielding good estimates of the maximum shear stress (errors smaller than 15% in all cases). The minimum shear stress is accurately predicted (errors smaller than 3%) for the non-skewed waves (Fig. 2), while it is underpredicted by as much as 30% for the strongly skewed waves (Fig. 4). However, in the strongly skewed cases, the minimum shear stress has a much smaller magnitude than the maximum, and the net sediment transport is onshore dominated. Thus, the error in the negative stresses does not undermine the model's ability to predict net sediment transport. The two models' predictions of the lag between the maximum near-bed velocity (indicated in the figures by a tick mark on the time axis) and the maximum bed shear stress differ by less than $T/50$.

Figs. 3 and 4 show disagreement between the shear stress predictions of the numerical and conceptual models in the neighborhood of the zero down-crossing flow velocity. The case where the disagreement is most pronounced (As=0.25, Sk=0.50, and k_N=1 mm in Fig. 4) is enlarged in Fig. 5. This disagreement is due to the sudden increase of flow acceleration at point P (see Fig. 5). Physically, the dynamics of the boundary layer before P are governed by the quasi-sinusoidal velocity profile between C and P and are not affected by the acceleration increase at P, as the numerical model reproduces. In contrast, the conceptual model calculates the shear stress shortly before P based on the near-bed velocity shortly after P, due to the phase lag between shear stress and velocity. Thus, the shear stress is underpredicted. To obtain an accurate prediction of the shear stress before P, (7) should not be applied based on the real velocity between P and E, but on a fictitious velocity that extends the quasi-sinusoidal profile between C and P, as represented by the dotted line between P and E'. However, as noted above, this inaccuracy in the negative shear stress computations has a negligible influence on net sediment transport predictions.

The agreement between the numerical and conceptual models remains good when the numerical model is started from rest (with small, consistent initial values of the variables) and run for half a

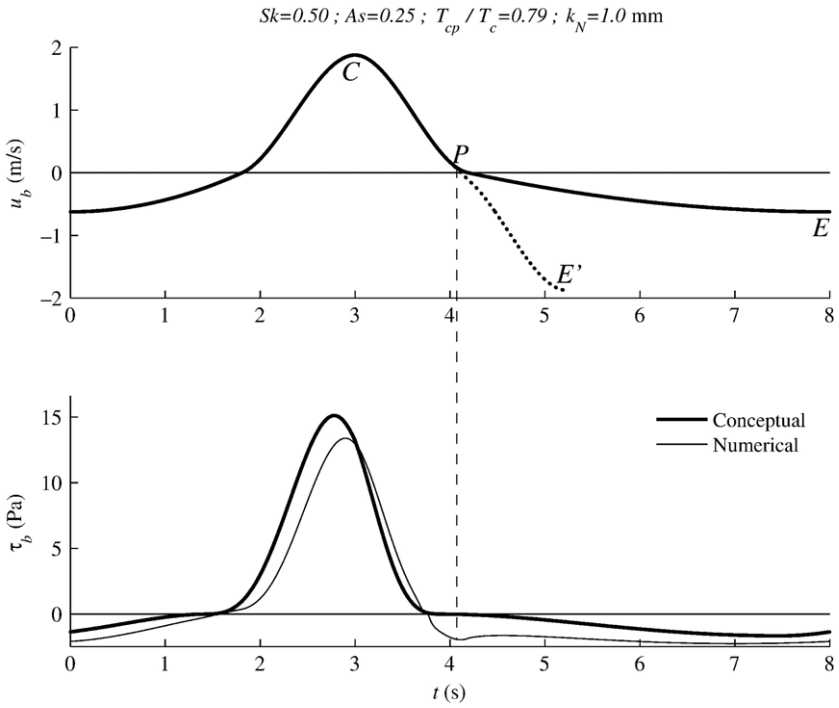

Fig. 5. Top: near-bed wave orbital velocity for the $As=0.25$, $Sk=0.50$, and $k_N=1$ mm case in Fig. 4. Bottom: disagreement between shear stress predictions from the conceptual (thick line) and numerical (thin line) models.

wave cycle. This justifies the application of the conceptual model to predict the bed shear stresses due to a half wave in Section 4 (experimental conditions of King, 1991, and of Hassan and Ribberink, 2005, series Q). Fig. 6 shows the temporal variation of bed shear stress predicted by the numerical model for the case with $As=0.33$, $Sk=0.33$, and $k_N=1$ mm. The dashed line is obtained when the model is started from rest and run for only one wave period. The solid line is obtained when the model is run until the results exhibit a periodic behavior. The maximum shear stress predictions differ by 7%, and the predictions of the time-integral of the onshore bed shear stresses to the 3/2 power (an estimate of the onshore bedload) differ by 14%. When

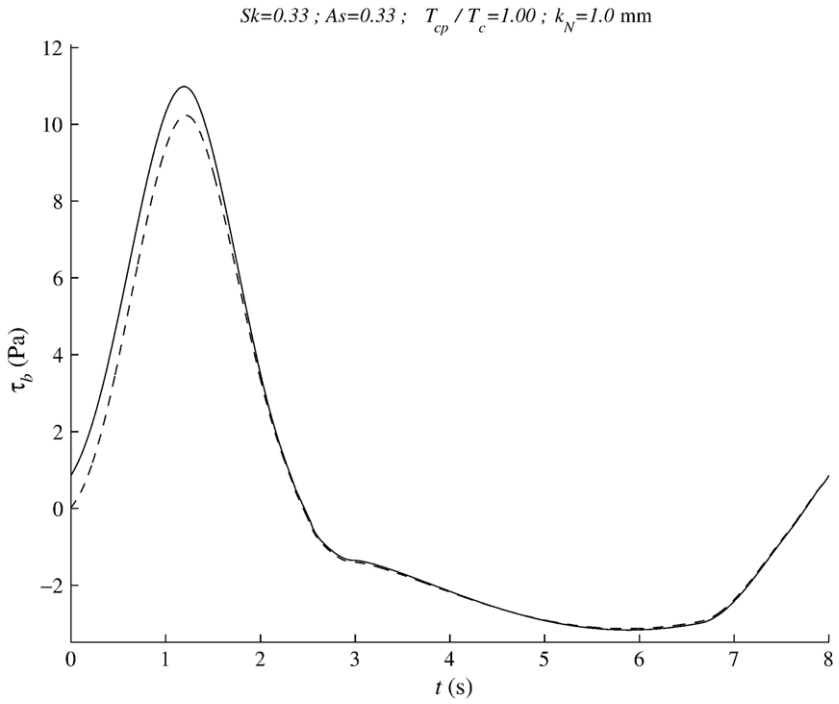

Fig. 6. Bed shear stresses predicted by the first iteration of the numerical model started from rest (dashed line) and once the results become periodic (solid line).

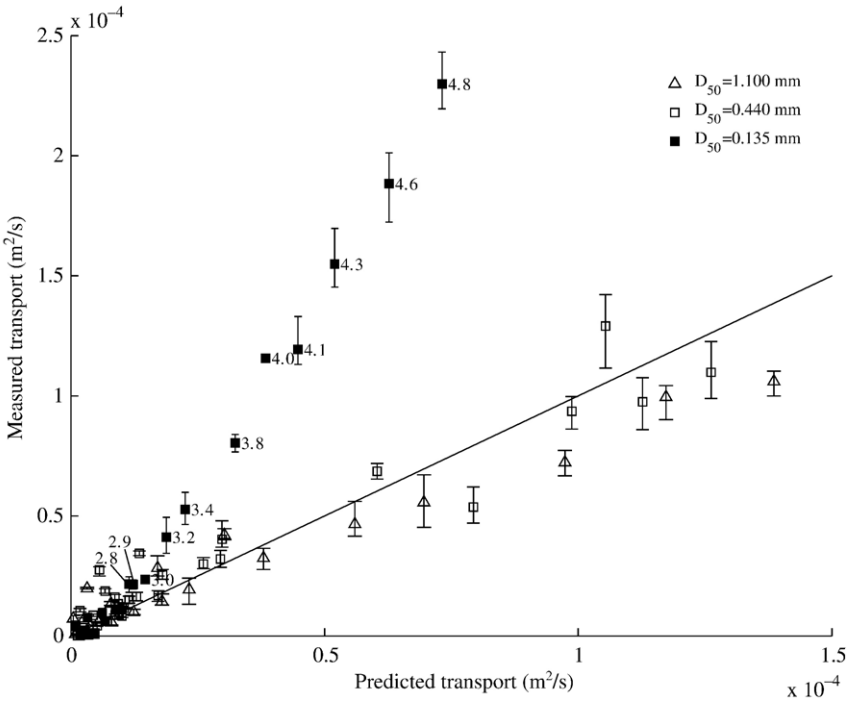

Fig. 7. Comparison between measured (King, 1991) and predicted average sediment transport rates over half a sinusoidal wave period. Vertical bars reflect the range of reported measurements. The values of u_{*m}/w_s are indicated for those cases with $u_{*m}/w_s>2.7$. The line of perfect agreement is shown.

suspension effects are negligible the sediment responds almost instantaneously to the flow (Madsen, 1991) even for sheet flow conditions (O'Donoghue and Wright, 2004, Fig. 10). Therefore, the accurate estimation of the instantaneous bed shear stresses by the conceptual model indicates its applicability to predict bedload transport for both half- and full-cycle (periodic) waves.

4. Prediction of bedload transport

To predict sheet flow bedload transport, we use the formula developed by Madsen (1991, 1993), which is based on a conceptualization of the mechanics of sediment transport and is similar in form to the empirical Meyer-Peter and Müller (1948) formula. Madsen (1993) generalized his 1991 bedload formula to a sloping bed; the derivation is reproduced in Appendix A for the reader's convenience. According to Madsen (1993), the instantaneous bedload sediment transport rate in a two-dimensional flow over a sloping bed is

$$q_{SB}(t)=\frac{8}{(s-1)\rho g}\max\left[0,|\tau_b(t)|-\tau_{cr,\beta}\right]\frac{\left(\sqrt{|\tau_b(t)|/\rho}-\alpha_\beta\sqrt{\tau_{cr,\beta}/\rho}\right)}{\cos\beta(\tan\phi_m+\tan\beta)}\frac{\tau_b(t)}{|\tau_b(t)|}, \tag{29}$$

where q_{SB} (t) is the volume of sediment transported per unit time and width, β is the bottom slope in the direction of transport, taken positive if sediment is transported upslope, $s=\rho_s/\rho$ is the ratio between sediment and water densities, $\tau_{cr,\beta}$ and α_β are given by (A.6) and (A.10), respectively, and $\phi_s\approx 50°$ and $\phi_m\approx 30°$ are the values of the angles of static and moving friction recommended by Madsen (2001). The bed shear stress, $\tau_b(t)$, is calculated using the conceptual model with $k_N=D_{50}$. This is consistent with the roughness value used to compute the fluid drag forces in the derivation of (29), presented in Appendix A. Previous studies have shown that the total hydraulic roughness that parameterizes the sheet flow velocity profile is larger than D_{50} (e.g., Dohmen-Janssen et al., 2001; Hsu et al., 2006). Here, $k_N=D_{50}$ is applied to calculate the effective bed shear stress that is responsible for sediment transport, which is only a fraction of the total bed shear stress. The use of an effective bed shear stress based on $k_N=D_{50}$ has previously been shown to yield good predictions of bedload over both plane and rippled beds for pure wave motion (Madsen and Grant, 1976). This is also the case for pure wave sheet flow conditions, provided that the maximum Shields parameter, ψ_m, is smaller than about 2 (Ribberink, 1998), as it is for all the bedload-dominated measurements considered in this paper. The appropriate value of k_N to predict sediment transport for strong oscillatory sheet flow ($\psi_m>2$) remains an open question, due to the scarcity of oscillatory sheet flow transport data in this range.

Laboratory studies of sediment transport under sheet flow conditions, the dominant bed regime in the nearshore region, have focused on skewed, symmetric waves (e.g., Ribberink and Al-Salem, 1994; Dohmen-Janssen and Hanes, 2002; Ahmed and Sato, 2003; O'Donoghue and Wright, 2004; Hassan and Ribberink, 2005). While waves in the surf zone are strongly asymmetric, only a few laboratory studies (King, 1991; Watanabe and Sato, 2004) have investigated asymmetric waves. King (1991) measured average sediment transport rates over half a period (from zero up-crossing to zero down-crossing near-bed velocity) of sinusoidal and asymmetric

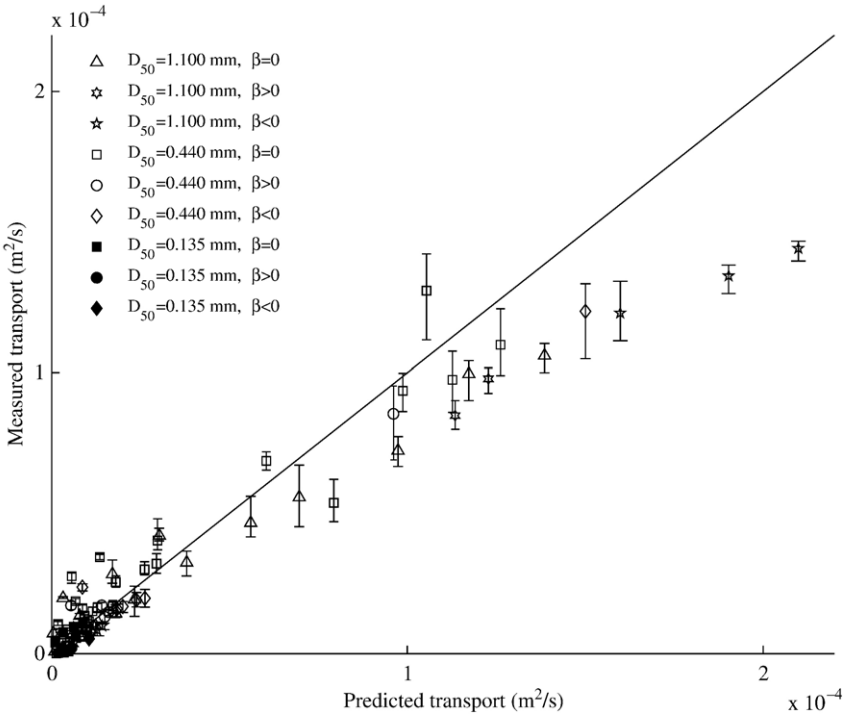

Fig. 8. Comparison between measured (King, 1991) and predicted average sediment transport rates over half a sinusoidal wave period for bedload-dominated cases ($u_{*m}/w_s<2.7$). The bed was horizontal ($\beta=0$), upslope in the direction of transport ($\beta>0$), or downslope in the direction of transport ($\beta<0$). Vertical bars reflect the range of reported measurements. The line of perfect agreement is shown.

waves, whereas all the other studies measured average sediment transport rates over the whole wave period.

Fig. 7 shows a comparison between predictions of average sediment transport rates by our conceptual model and oscillatory wave tunnel measurements for sinusoidal waves by King (1991). King's experiments were run for half a wave cycle and the measured sediment transport rates correspond to onshore wave velocities only. The average transport predictions are based on the bed shear stress predicted by the conceptual model using the half-wave near-bed velocity profiles inferred from the piston motion and $k_N=D_{50}$. Note that, for sinusoidal waves, the conceptual model for bed shear stress reduces to that of Madsen (1994). Predictions and measurements agree for the coarse and medium grain cases ($D_{50}=1.1$ and 0.44 mm), demonstrating the predictive ability of the bedload formula, (29). The disagreement between predictions and measurements for some of the fine grain cases ($D_{50}=0.135$ mm) is attributed to suspension effects, which are not accounted for by the bedload formula.

The importance of suspension effects is quantified by the ratio between the settling time of a suspended particle, δ/w_s, and the wave period, T. δ is a typical entrainment height and w_s is the settling velocity, calculated using Jiménez and Madsen's (2003) formula. Particle entrainment is governed by the advection-diffusion equation, in which the time scales as T and the eddy viscosity scales as $\kappa u_{*m} z$, where u_{*m} is the maximum shear velocity and z is the vertical distance from the boundary. This implies that δ scales as $\kappa u_{*m} T$ (i.e., δ is of the same order as the wave boundary layer thickness). Suspension effects become important when $\delta/(w_s T)$ is larger than about 1 or, equivalently, when u_{*m}/w_s is larger than about 2.5. The conceptual model predicts $u_{*m}/w_s \approx 0.2$–1.2 for King's coarse and medium grain cases and $u_{*m}/w_s \approx 1.6$–4.8 for King's fine grain cases. These values confirm that suspension effects are more relevant in the latter. Within the fine grain cases, those with $u_{*m}/w_s<2.7$ are well predicted by the bedload formula, while those with $u_{*m}/w_s>2.7$—for which the values of u_{*m}/w_s are indicated in Fig. 7—are underpredicted. Thus, we take $u_{*m}/w_s \approx 2.7$ as the threshold above which sediment suspension effects become important. Note that the deviation from the 1:1 line of the data points with $u_{*m}/w_s>2.7$ systematically increases as u_{*m}/w_s increases, suggesting that this parameter correctly quantifies the importance of suspended transport. Since King's measurements correspond to onshore wave velocities only, the suspended transport is necessarily directed onshore, and the measurements with $u_{*m}/w_s>2.7$ are underpredicted. In contrast, suspended transport under full periodic waves is not necessarily directed onshore, as will be discussed in Section 5.

A similar parameter to account for the importance of suspended sediment phase lag effects was proposed by Dohmen-Janssen et al. (2002). When their parameter exceeds a certain threshold, Dohmen-Janssen et al. anticipate phase lag effects to become important, which is analogous to our criterion for rejection of data due to suspension effects. In contrast with our study, Dohmen-Janssen et al. assume that the entrainment height δ scales as the sheet flow layer thickness. Nevertheless, out of the 217 experimental conditions considered in this paper, all 161 cases that our criterion classifies as bedload dominated also correspond to negligible phase lag effects according to Dohmen-Janssen et al.'s criterion. Of the remaining 56 cases

rejected by our criterion, 23 would have also been rejected by Dohmen-Janssen et al.'s.

Fig. 8 shows the same comparison as Fig. 7, but including measurements with positive and negative bottom slopes. Only measurements with $u_{*m}/w_s<2.7$ are plotted. The bedload formula successfully captures slope effects, although it tends to overpredict the largest transport rates. The small negative bias for the largest transport rates may be due to sand being transported over the trap, as noted by King (1991).

Fig. 9 shows a comparison between predictions of average sediment transport rates by our conceptual model and oscillatory wave tunnel measurements by Ribberink and Al-Salem (1994, series B, cases 7–16), Ahmed and Sato (2003, cases U1–U13 and U15), O'Donoghue and Wright (2004, series MA and CA), and Hassan and Ribberink (2005, series R and Q). In the experiments, the near-bed orbital velocity is symmetric ($As=0$) but skewed ($0.13<Sk<0.31$). The bed remained flat. All studies measured average transport rates over the entire wave cycle, with the exception of Hassan and Ribberink's (2005) series Q, in which the onshore and offshore transport components over half-wave cycles were measured separately. The measured average (net) transport rates used for series Q by Hassan and Ribberink (2005) are calculated from the onshore and offshore transport rates reported in their Table 5, since the net transport rates in the last column of the table are incorrect (Ribberink and Hassan, personal communication, 2007). In addition, their measured onshore transport rates significantly differ from the transport rates measured by King (1991) under similar conditions. Our model's predictions are based on the wave velocities inferred from the movement of the wave piston. For Ahmed and Sato's experiments, we use the near-bed velocity time-series provided by the authors (Ahmed, personal communication, 2006). For all other cases, the near-bed velocities are modeled as second-order Stokes waves. Only those measurements for which the conceptual model predicts $u_{*m}/w_s<2.7$ are shown in Fig. 9. The conceptual model yields a good agreement with these measurements, for which bedload is the dominant transport mechanism.

Figs. 10 and 11 show comparisons between predictions of the average sediment transport rate by our conceptual model and measurements from experiments with asymmetric and non-skewed ($Sk=0$) waves conducted in oscillatory water tunnels by King (1991, steep front and steep rear wave series, $As=\pm0.56$) and Watanabe and Sato (2004, cases 1–33, $0.10<As<0.36$). King's runs are forward- and backward-leaning half waves, consisting of a forward stroke of the wave maker. In contrast, Watanabe and Sato simulated the complete oscillatory motion and measured the average transport rate over the entire wave cycle under forward-leaning waves. The numerical values of Watanabe and Sato's data are reported by Nielsen (2006, Appendix B). Again, our model's predictions are based on the wave velocities inferred from the movement of the wave piston. Only bedload-dominated cases, for which the conceptual model predicts $u_{*m}/w_s<2.7$, are included in Figs. 10 and 11. The conceptual model predictions agree well with King's half-wave transport data (shown in detail in Fig. 11), which include forward- and backward-leaning half waves. In contrast, the model underpredicts most of Watanabe and Sato's average transport data (Fig. 10). It is noted that Watanabe and Sato's coarse grain data (cases 16–21, numbered in Fig. 10) show unexpected patterns that make their reliability questionable. Specifically, although case 19 has a velocity amplitude 50%

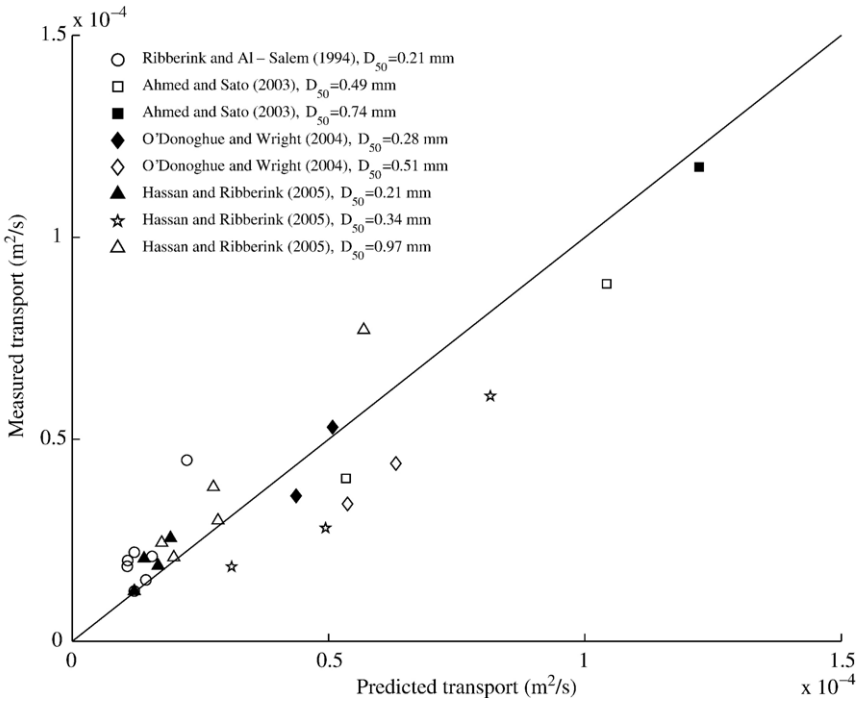

Fig. 9. Comparison between measured and predicted average sediment transport rates under skewed, symmetric waves ($Sk>0$, $As=0$) for bedload-dominated cases ($u_{*m}/w_s<2.7$). The line of perfect agreement is shown.

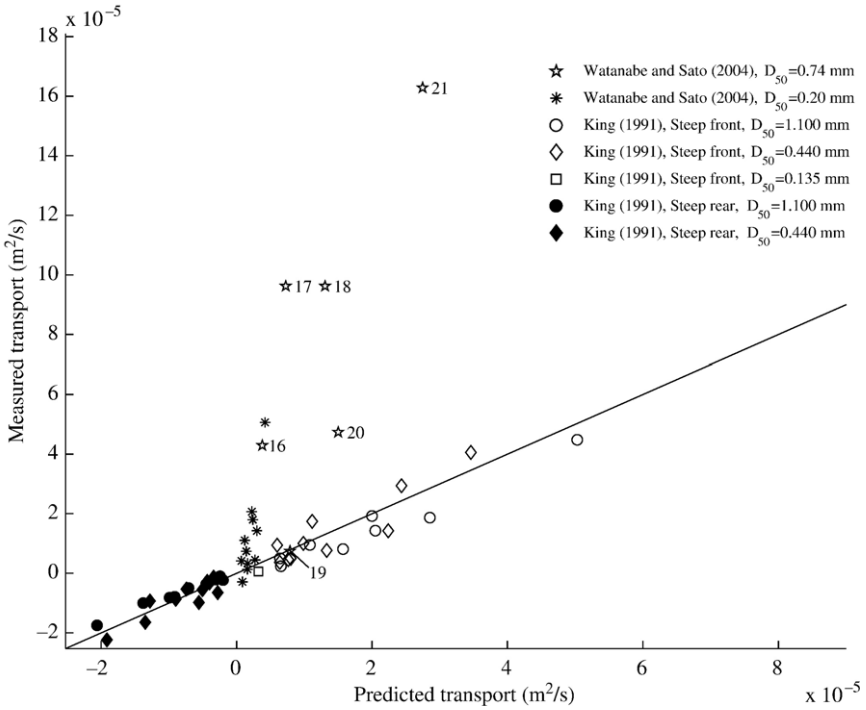

Fig. 10. Comparison between measured and predicted average sediment transport rates under asymmetric, non-skewed waves ($|As|>0$, $Sk=0$) for bedload-dominated cases ($u_{*m}/w_s<2.7$). The average transport rate under King's forward-leaning half waves (which correspond to onshore velocities) is represented as a positive value, while the average transport rate under King's backward-leaning half waves (which correspond to offshore velocities) is represented as a negative value. Case numbers for Watanabe and Sato's (2004) coarse grain data are indicated. The line of perfect agreement is shown.

larger than case 16 (all other parameters being equal), the measured transport rate in case 19 is 5 times smaller. Similarly, the conditions in cases 17 and 18 differ only in the significantly larger asymmetry of the latter ($As=0.20$ and 0.36, respectively), in spite of which the measured net transport rates are virtually identical. Most of Watanabe and Sato's fine grain cases are not

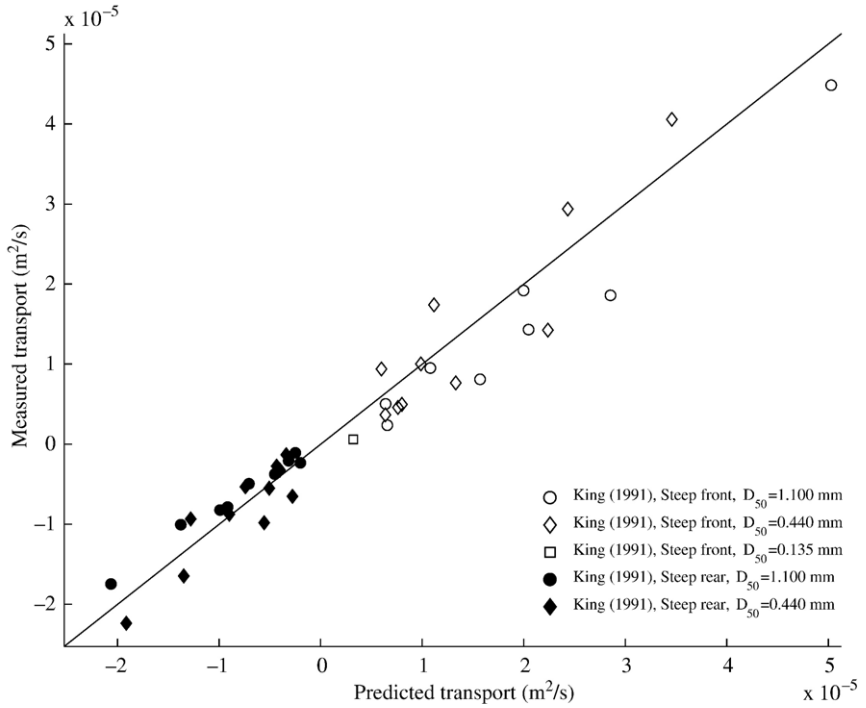

Fig. 11. Comparison between measured and predicted average sediment transport rates under asymmetric, non-skewed waves (King, 1991) for bedload-dominated cases ($u_{*m}/w_s<2.7$). See also caption to Fig. 10.

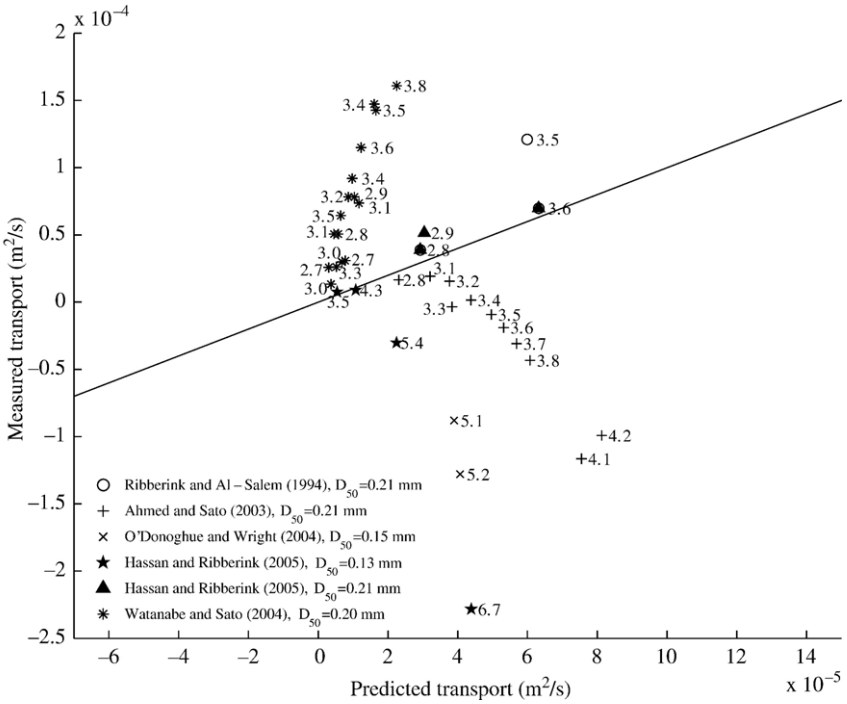

Fig. 12. Comparison between measured and predicted average sediment transport rates under skewed waves and asymmetric waves for cases where a significant contribution of suspended transport is expected. Values of $u_{*m}/w_s > 2.7$ are indicated. The line of perfect agreement is shown.

presented in Fig. 10, since significant suspended transport is expected ($u_{*m}/w_s > 2.7$). It is noted that the inconsistency of Watanabe and Sato's coarse grain data and the strong contribution of suspended transport in most of the fine grain cases suggest that the calibration of Nielsen's (2006) bedload transport model parameter against Watanabe and Sato's (2004) dataset may be inappropriate.

In summary, the conceptual model for computing bed shear stress has been successfully applied to predict bedload under skewed wave conditions and under asymmetric wave conditions. It is noted that the only consistent, bedload-dominated sediment transport laboratory data available under asymmetric, periodic waves are, to the authors' knowledge, the measurements by King (1991). Therefore, while the predictive ability of the bed shear stress model and its application to compute bedload under asymmetric waves seems promising, more experimental data are necessary for further verification of the model.

5. Suspended transport effects

When suspension effects are negligible (i.e., when $u_{*m}/w_s < 2.7$), the bedload formula (29) successfully predicts the total transport. When suspension effects become important (i.e., when $u_{*m}/w_s > 2.7$), the total transport rate differs from the bedload transport, which, by analogy with the previous case, is assumed to be given by (29). We investigate the qualitative effects of suspension under asymmetric and skewed waves by comparing our bedload predictions with measurements of total transport. Fig. 12 shows a comparison between predicted and measured average transport rates under asymmetric waves (data of Watanabe and Sato, 2004) and skewed waves (all other data). The figure only includes those cases with significant sediment suspension, for which the values of u_{*m}/w_s are indicated. Again, the deviation of the data points from the 1:1 line systematically increases with the value of u_{*m}/w_s. This is most clearly evidenced by Ahmed and Sato's 0.21 mm cases (+), suggesting that u_{*m}/w_s correctly quantifies the importance of suspended transport. As shown in the figure, the skewed wave data are overpredicted by the bedload model and the asymmetric wave data are underpredicted. This suggests that suspended transport reduces the total onshore transport under skewed waves and increases the total onshore transport under asymmetric waves. In a skewed, symmetric wave, shortly after the large shear stress around the near-bed velocity crest puts sediment in suspension, the near-bed velocity turns negative and transports the sediment offshore. This effect has been discussed by Hassan and Ribberink (2005) for skewed waves, and previously by Dohmen-Janssen et al. (2002) in the context of sinusoidal waves superimposed on a current. Since our sediment transport formula does not account for sediment in suspension, it overpredicts the net transport rates for the skewed wave cases where suspended transport is significant. In contrast, suspended sediment transport under asymmetric, non-skewed waves appears to increase the total transport. In an asymmetric, non-skewed wave, the near-bed velocity is directed onshore for a relatively long time after the crest. Thus, the sediment suspended by the large shear stress near the crest stays in suspension while the velocity is directed onshore. This phenomenon was observed experimentally by Watanabe and Sato (2004), as shown in their Fig. 5. Note that, in an asymmetric, non-skewed wave, the shear stress at the trough has

a smaller magnitude than the shear stress at the crest. Consequently, the suspended transport yields a net onshore contribution, which is not accounted for by the bedload formula, (29), and leads to underprediction of Watanabe and Sato's 0.20 mm cases in Fig. 12.

6. Conclusion

We developed a simple model for the bed shear stress that extends the classic sinusoidal wave theory to asymmetric and skewed waves. Our model uses a time-variable friction factor that accounts for the variability in wave shape. The near-bed velocity profile between the zero up-crossing and the crest is approximated by a quarter of a sinusoid, which provides an estimate of the friction factor at the crest. The friction factor at the trough is estimated analogously. Then, a linear friction factor variation between the crest and trough values is assumed. The computations of bed shear stress by the conceptual model compare favorably with the results of a numerical boundary layer model with a k–ε turbulence closure. The bed shear stress model is readily applicable to predict bedload sediment transport. In contrast with the approaches of Hoefel and Elgar (2003) and Nielsen (2006) to compute sediment transport, we do not parameterize the effect of fluid acceleration or the horizontal pressure gradients acting on the sediment particles. Rather, we calculate sediment transport from the bed shear stress, obtained as a function of the near-bed wave velocity, as was previously done by Henderson et al. (2004) to predict nearshore sandbar migration. Unlike Hoefel and Elgar's (2003) and Nielsen's (2006) formulations, our methodology for computing bedload under asymmetric and skewed waves relies on physically based mechanistic arguments, and it is free of adjustable parameters. Bedload predictions agree with laboratory measurements of sheet flow under asymmetric waves and skewed waves in those cases where bedload is the dominant transport mechanism. However, the number of studies of sheet flow bedload under asymmetric waves available to date is insufficient for definitive verification of our model. Based on the comparison with the numerical model, it is expected that our conceptual model will also be able to predict bedload transport under waves that are both asymmetric and skewed, for which no experimental data appear available.

When sediment suspension becomes relevant, phase lags between concentration of suspended sediment and near-bed orbital velocity become important. As shown in experiments, the effect of sediment suspension on net transport depends on wave shape. In asymmetric waves, after the steep wave front causes the largest sediment suspension, the velocity remains directed onshore for a rather long time, and the suspended transport is directed onshore. In skewed waves, due to the narrower wave crest, the velocity turns offshore shortly after the largest sediment suspension occurs, and the suspended transport may potentially be directed offshore. Since the bed shear stress model presented here successfully predicts the phase lag between bed shear stress and near-bed velocity, we anticipate its applicability to the prediction of total (bedload and suspended) net sediment transport under asymmetric and skewed waves.

Acknowledgments

The support of the Office of Naval Research, Coastal Geosciences Program under Grant Number N00014-6-1-0318 is gratefully acknowledged. The authors wish to thank Drs. Ahmed Ahmed, Wael Hassan, David King, Jan Ribberink, Shinji Sato, and Akira Watanabe for providing unpublished details of their experimental data.

Appendix A. Bedload transport on a sloping bed (Madsen, 1993)

Consider a plane bed inclined at an angle β to horizontal in the direction of transport, where β is taken positive if sloping upward in the direction of transport. At the point of incipient sediment motion, the force balance between drag, gravity, and frictional resistance against movement yields

$$\frac{1}{2}\rho C_D\left(\frac{\pi}{4}d^2\right)u_{cr,\beta}^2-(\rho_s-\rho)g\left(\frac{\pi}{6}d^3\right)\sin\beta = (\rho_s-\rho)g\left(\frac{\pi}{6}d^3\right)\cos\beta\tan\phi_s, \tag{A.1}$$

where C_D and ϕ_s are the drag coefficient and friction angle, respectively, for a stationary superficial grain, which is assumed spherical in shape, of diameter d and density ρ_s. $u_{cr,\beta}$ is a representative critical velocity for initiation of motion used in the evaluation of the drag force, and ρ is the water density. Rearranging (A.1) yields

$$\frac{u_{cr,\beta}^2}{(s-1)gd}=\frac{4}{3C_D}\tan\phi_s\left[\cos\beta\left(1+\frac{\tan\beta}{\tan\phi_s}\right)\right]. \tag{A.2}$$

For a sediment grain rolling or sliding along the inclined bed, the balance of fluid drag, gravity, and frictional forces yields

$$\frac{1}{2}\rho C_D\left(\frac{\pi}{4}d^2\right)\left(u_f-u_s\right)^2-(\rho_s-\rho)g\left(\frac{\pi}{6}d^3\right)\sin\beta = (\rho_s-\rho)g\left(\frac{\pi}{6}d^3\right)\cos\beta\tan\phi_m, \tag{A.3}$$

where u_f is a characteristic fluid velocity, u_s is the velocity of the sediment grain, and ϕ_m is the angle of moving friction. Rearranging (A.3) yields

$$\frac{\left(u_f-u_s\right)^2}{(s-1)gd}=\frac{4}{3C_D}\tan\phi_m\left[\cos\beta\left(1+\frac{\tan\beta}{\tan\phi_m}\right)\right]. \tag{A.4}$$

Combining (A.2) and (A.4) results in the following expression for the sediment grain velocity

$$u_s=u_f-u_{cr,\beta}\sqrt{\frac{\tan\phi_m+\tan\beta}{\tan\phi_s+\tan\beta}} \tag{A.5}$$

when the drag coefficients are assumed equal.

The immobile sediment grains on the bottom can support the critical shear stress for initiation of motion,

$$\tau_{cr,\beta} = \tau_{cr,0}\left[\cos\beta\left(1+\frac{\tan\beta}{\tan\phi_s}\right)\right], \tag{A.6}$$

where $\tau_{cr,0}$ is determined using the Shields diagram (e.g., Madsen, 2001). Since sediment is moving, the excess skin friction shear stress, $|\tau_b|-\tau_{cr,\beta}>0$, must be carried by moving grains. The fluid drag force on a moving grain, $F_{D,m}$, is given by the first term in (A.3). Denoting the number of grains in motion per unit area by N, this argument leads to

$$\begin{aligned}|\tau_b| - \tau_{cr,\beta} &= NF_{D,m}\\ &= \left\{N\frac{\pi}{6}d^3\right\}(s-1)\rho g\cos\beta\tan\phi_m\left(1+\frac{\tan\beta}{\tan\phi_m}\right).\end{aligned} \tag{A.7}$$

The term in {} represents the sediment volume in motion per unit area. With the velocity of the sediment in motion given by (A.5), the bedload transport rate, q_{SB}, is

$$\begin{aligned}q_{SB} = N\left(\frac{\pi}{6}d^3\right)u_s = \frac{\left(|\tau_b|-\tau_{cr,\beta}\right)}{(s-1)\rho g\cos\beta(\tan\phi_m+\tan\beta)}\\ \left(u_f - u_{cr,\beta}\sqrt{\frac{\tan\phi_m+\tan\beta}{\tan\phi_s+\tan\beta}}\right)\end{aligned} \tag{A.8}$$

if $|\tau_b|>\tau_{cr,\beta}$ and 0 otherwise. Following Madsen (1991), the reference fluid velocities u_f and $u_{cr,\beta}$, used in calculating fluid drag forces, are based on $k_N=D_{50}$ and evaluated from the log-profile at $z=0.8D_{50}$. Introducing these reference velocities into (A.8) yields

$$\begin{aligned}q_{SB}(t) = \frac{8}{(s-1)\rho g}\max\left[0,|\tau_b(t)|-\tau_{cr,\beta}\right]\\ \frac{\left(\sqrt{|\tau_b(t)|/\rho}-\alpha_\beta\sqrt{\tau_{cr,\beta}/\rho}\right)}{\cos\beta(\tan\phi_m+\tan\beta)}\frac{\tau_b(t)}{|\tau_b(t)|},\end{aligned} \tag{A.9}$$

where

$$\alpha_\beta = \sqrt{\frac{\tan\phi_m+\tan\beta}{\tan\phi_s+\tan\beta}}. \tag{A.10}$$

References

Ahmed, A.S.M., Sato, S., 2003. A sheetflow transport model for asymmetric oscillatory flows. Part I: uniform grain size sediments. Coastal Engineering Journal 45 (3), 321–337.

Bailard, J.A., 1981. An energetics total load sediment transport model for a plane sloping beach. Journal of Geophysical Research 86 (C11), 10938–10954.

Calantoni, J., Puleo, J.A., 2006. Role of pressure gradients in sheet flow of coarse sediments under sawtooth waves. Journal of Geophysical Research 111 (C01010). doi:10.1029/2005JC002875.

Davies, A.G., Soulsby, R.L., King, H.L., 1988. A numerical model of the combined wave and current bottom boundary layer. Journal of Geophysical Research 93 (C1), 491–508.

Dohmen-Janssen, C.M., Hanes, D.M., 2002. Sheet flow dynamics under monochromatic nonbreaking waves. Journal of Geophysical Research 107 (C10), 3149. doi:10.1029/2001JC001045.

Dohmen-Janssen, C.M., Hassan, W.N., Ribberink, J.S., 2001. Mobile-bed effects in oscillatory sheet flow. Journal of Geophysical Research 106 (C11), 27103–27115.

Dohmen-Janssen, C.M., Kroekenstoel, D.F., Hassan, W.N., Ribberink, J.S., 2002. Phase lags in oscillatory sheet flow: experiments and bed load modelling. Coastal Engineering 46, 61–87.

Drake, T.G., Calantoni, J., 2001. Discrete particle model for sheet flow sediment transport in the nearshore. Journal of Geophysical Research 106 (C9), 19859–19868.

Einstein, H.A., 1950. The Bed-load Function for Sediment Transportation in Open Channel Flows. Technical Bulletin, vol. 1026. U. S. Department of Agriculture, Soil Conservation Service.

Elfrink, B., Hanes, D.M., Ruessink, B.G., 2006. Parameterization and simulation of near bed orbital velocities under irregular waves in shallow water. Coastal Engineering 53, 915–927.

Engelund, F., Hansen, E., 1967. A Monograph on Sediment Transport in Alluvial Streams. Teknisk Forlag, Copenhagen.

Evans, G., Blackledge, J., Yardley, P., 2000. Numerical Methods for Partial Differential Equations, 1st edition. Springer Undergraduate Mathematics Series. Springer.

Hamilton, D.G., Ebersole, B.A., 2001. Establishing uniform longshore currents in a large-scale sediment transport facility. Coastal Engineering 42, 199–218.

Hassan, W.N., Ribberink, J.S., 2005. Transport processes of uniform and mixed sands in oscillatory sheet flow. Coastal Engineering 52, 745–770.

Henderson, S.M., Allen, J.S., Newberger, P.A., 2004. Nearshore sandbar migration predicted by an eddy-diffusive boundary layer model. Journal of Geophysical Research 109 (C06024). doi:10.1029/2003JC002137.

Hoefel, F., Elgar, S., 2003. Wave-induced sediment transport and sandbar migration. Science 299, 1885–1887.

Holmedal, L.E., Myrhaug, D., 2006. Boundary layer flow and net sediment transport beneath asymmetrical waves. Continental Shelf Research 26, 252–268.

Holmedal, L.E., Myrhaug, D., Rue, H., 2003. The sea bed boundary layer under random waves plus current. Continental Shelf Research 23, 717–750.

Hsu, T.-J., Hanes, D.M., 2004. Effects of wave shape on sheet flow sediment transport. Journal of Geophysical Research 109 (C05025). doi:10.1029/2003JC002075.

Hsu, T.-J., Elgar, S., Guza, R.T., 2006. Wave-induced sediment transport and onshore sandbar migration. Coastal Engineering 53, 817–824.

Jiménez, J.A., Madsen, O.S., 2003. A simple formula to estimate settling velocity of natural sediments. Journal of Waterway, Port, Coastal and Ocean Engineering 129 (2), 70–78.

Jonsson, I.G., 1966. Wave boundary layers and friction factors. Proceedings of the 10th International Conference on Coastal Engineering. ASCE, pp. 127–148.

Justesen, P., 1988. Prediction of turbulent oscillatory flow over rough beds. Coastal Engineering 12, 257–284.

King, D.B., 1991. Studies in oscillatory flow bedload sediment transport. Ph.D. thesis, University of California, San Diego.

Launder, B.E., Spalding, D.B., 1974. The numerical computation of turbulent flows. Computer Methods in Applied Mechanics and Engineering 3, 269–289.

Liu, H., Sato, S., 2006. A two-phase flow model for asymmetric sheetflow conditions. Coastal Engineering 53, 825–843.

Madsen, O.S., 1991. Mechanics of cohesionless sediment transport in coastal waters. Proceedings of Coastal Sediments '91. ASCE, pp. 15–27.

Madsen, O.S., 1993. Sediment Transport Outside the Surf Zone. Technical Report. U.S. Army Engineer Waterways Experiment Station, Vicksburg, MS.

Madsen, O.S., 1994. Spectral wave-current bottom boundary layer flows. Proceedings of the 24th International Conference on Coastal Engineering. ASCE, pp. 384–398.

Madsen, O.S., 2001. Sediment transport outside the surf zone. Coastal Engineering Manual, vol. III. U.S. Army Corps of Engineers, Washington DC. Chapter 6.

Madsen, O.S., Grant, W.D., 1976. Quantitative description of sediment transport by waves. Proceedings of the 15th International Conference on Coastal Engineering. ASCE, pp. 1093–1112.

Madsen, O.S., Salles, P., 1998. Eddy viscosity models for wave boundary layers. Proceedings of the 26th International Conference on Coastal Engineering. ASCE, pp. 2615–2627.

Meyer-Peter, E., Müller, R., 1948. Formulas for bed-load transport. Proceedings of the 2nd Meeting of the International Association for Hydraulic Structures Research, pp. 39–64.

Nielsen, P., 1992. Coastal Bottom Boundary Layers and Sediment Transport. Advanced Series on Ocean Engineering, vol. 4. World Scientific.

Nielsen, P., 2002. Shear stress and sediment transport calculations for swash zone modelling. Coastal Engineering 45, 53–60.

Nielsen, P., 2006. Sheet flow sediment transport under waves with acceleration skewness and boundary layer streaming. Coastal Engineering 53, 749–758.

Nielsen, P., Callaghan, D.P., 2003. Shear stress and sediment transport calculations for sheet flow under waves. Coastal Engineering 47, 347–354.

O'Donoghue, T., Wright, S., 2004. Flow tunnel measurements of velocities and sand flux in oscillatory sheet flow for well-sorted and graded sands. Coastal Engineering 51, 1163–1184.

Pope, S.B., 2000. Turbulent Flows, 1st edition. Cambridge University Press.

Press, W.H., Teukolsky, S.A., Vetterling, W.T., Flannery, B.P., 1992. Numerical Recipes in Fortran 77. The Art of Scientific Computing, 2nd edition. Cambridge University Press.

Ribberink, J.S., 1998. Bed-load transport for steady flows and unsteady oscillatory flows. Coastal Engineering 34, 59–82.

Ribberink, J.S., Al-Salem, A.A., 1994. Sediment transport in oscillatory boundary layers in cases of rippled beds and sheet flow. Journal of Geophysical Research 99 (C6), 12707–12727.

Tajima, Y., Madsen, O.S., 2002. Shoaling, breaking and broken wave characteristics. Proceedings of the 28th International Conference on Coastal Engineering. World Scientific, pp. 222–234.

Trowbridge, J., Madsen, O.S., 1984. Turbulent wave boundary layers. 1. Model formulation and first-order solution. Journal of Geophysical Research 89 (C5), 7989–7997.

Watanabe, A., Sato, S., 2004. A sheet-flow transport rate formula for asymmetric, forward-leaning waves and currents. Proceedings of the 29th International Conference on Coastal Engineering. World Scientific, pp. 1703–1714.